Identification of In Situ Frictional Properties of Bolted Assemblies with Digital Image Correlation

Jordan de Crevoisier, Nicolas Swiergiel, Laurent Champaney, François Hild

Experimental Mechanics manuscript No.
(will be inserted by the editor)

Identification of in situ frictional properties of bolted assemblies with digital image correlation

Jordan de Crevoisier · Nicolas Swiergiel · Laurent Champaney · François Hild

Received: date / Accepted: date

Abstract The present paper is devoted to the identification of frictional properties in bolted assemblies. It is shown that kinematic data provided by digital image correlation can be used to analyze the change of the friction coefficient with the number of cycles. Two approaches are followed. The first one is based on the displacement jump between the assembled plates, and the second one relies on displacement fields measured on the same surface.

Keywords Experiment · Fatigue · Friction · Kinematic measurements · Simulation · Tension

J. de Crevoisier, L. Champaney, F. Hild*
Laboratoire de Mécanique et Technologie (LMT-Cachan)
ENS de Cachan / CNRS / Université Paris 6 / PRES UniverSud Paris
61 Avenue du Président Wilson, F-94235 Cachan Cedex, France
*Corresponding author: hild@lmt.ens-cachan.fr
J. de Crevoisier, N. Swiergiel
[2]EADS-IW, 12 rue Pasteur, F-92152 Suresnes, France

1 Introduction

Nowadays, whether it is in aluminium, composite or hybrid structures (*e.g.,* aluminum-titanium/carbon epoxy), an important part of the overall cost of aerospace structures comes from the assembly cycle (*i.e.,* drilling + fasteners + shim + mastic + handling represents almost 30 % of the total cost). Aerodynamic parts must be assembled on sub-structures with fasteners, which represent a major item of expenditure. One of the objectives of the present paper is to identify joint parameters by analyzing experiments. Most of the proposed tests involve fatigue events on different assembly types in order to determine which assembly parameter of the joint is crucial for life-time duration. In the present case, an elementary junction (*i.e.,* with a single bolt) is analyzed.

The last decade has seen an increased activity concerning the analysis of the mechanical behavior of bolted joints. Different aspects have been discussed, namely, experimental, modeling, and both. Concerning the modeling side, there are three different types of approaches:

- A simplified model consists in describing the mechanical behavior of an assembly by a mass-spring system [1]. The stiffness of a unitary junction may follow Huth's formula [2]. These models enable for fast identifications of the transfer ratios in the considered assembly. Some of the models account for the clearance between the hole and the bolt [1]. A macro element [3] was also developed to account for global non-linearities in each bolted point.
- Alternative techniques based upon beam discretizations are also possible. They allow for a better description of the complex kinematics in a bolted assembly [4]. They are compared to 3D models in Ref. [5].
- The last and more involved analysis is a full three-dimensional description of the assembly. Different routes are followed. The first one corresponds to an averaged description of the material behavior [6] with the description of pre-loading and frictional properties within the assembly. In many instances, the behavior of the assembled elements remains elastic, even if elasto-plastic [7, 8] or damage [9] models have been considered. The stacking sequence of composites may also be explicitly

accounted for [1,10,11] and Hashin's criteria are used to evaluate ultimate properties. One of the key numerical issues is related to the contact between the bolt and the plates. Different commercial codes are used [6,8,11,12,13] to deal with this feature. A global / local scheme [14,15] is yet another way of accounting for contact properties in joints. In such models, many parameters (*e.g.,* friction coefficient, clearance) play a key role, yet their exact value is not known very accurately. Some dedicated strategies analyze the effects of such uncertainties [16,17].

These various models generally do not aim at evaluating the failure load after pre-load or after cycling. They enable for a better understanding of the behavior of different joints (*e.g.,* load transfer, friction versus bearing, role of bolt / hole clearance and pre-load, changes of the previous ones with the number of cycles). In terms of comparison with experiments [18,19,20], the same type of route is followed [1,7,8,10,11,18,19, 21,22,23]. Point data (*e.g.,* displacement, strain and/or load level [12,13,18,19]) are considered. This experimental database allows the authors to study the role of pre-load and the change of the frictional coefficient with the applied load [23,24,25]. However, no identification of parameters of the bolted junction are performed.

In terms of experimental instrumentation, four different quantities are usually measured [6,10,19,20,21,23,26,27]. Strains between bolts on one of the assembled plates are measured with strain gauges, the level of bolt tension is evaluated with strain gauges, the relative motion of two assembled plates plates or that between the bold head with respect to one of the plates is measured with extensometers. In the following study, Digital Image Correlation (DIC) is used to show its applicability to measuring displacement fields and analyzing the stiffness of bolted assemblies, and to study the change of the frictional coefficient with the applied number of cycles. FFT-DIC was used very recently to monitor local slip displacements between the specimen and pad in friction experiments by resorting to a long distance microscope [28]. In the present analysis, the observation will be on a larger scale.

The experimental procedure is presented in a first section. In particular, the full field measurement technique is validated against independent measurements. The second

section deals with the identification of the friction coefficient of three configurations in which the surface finish and the bolt tension are different. Only a global information is used, namely, the displacement jump between the central and external plates of the assembly. This analysis is subsequently validated in a third section in which measured and computed displacement fields are compared.

2 Experimental analyses

2.1 Studied specimen

The chosen configuration is a bolted assembly consisting of double lap joint with a single bolt (Figure 1) representative of aeronautical junctions. Two external plates made of 2024 T351 aluminum alloy (thickness: $e_a/2 = 4$ mm, width: 49.6 mm, length: 150 mm) are assembled with a central plate made of a layered carbon / epoxy composite (T700/M21, 32 layers, stacking sequence: (90/45/0/0/-45/0/0/45/0/-45/0/0/45/90/-45/0)s, width: $e_c = 8.32$ mm). Tabs made of glass fabric prepregs are glued onto the two faces of the composite plate to avoid premature failure in the grips. An aluminum alloy insert is put between the two external plates to allow for the use of classical grips. A width to hole diameter ratio of 5 is chosen. The aeronautic bolt (EN 6115T6-23 screw, ASNA 2531-6 nut, and NSA5379-6c washer) is made of titanium whose diameter is $D = 9.52$ mm (the clearance between the bolt of the various plates is of the order of 45 μm). The bolt tension is evaluated by a pressure cell. During the experiment, the tension T in the bolt is constantly measured. It is therefore possible to follow the level of normal force on the various plates.

2.2 Testing procedure

A servo-hydraulic testing machine is used to perform the experiments. The samples are loaded in tension with a constant load ratio for all the experiments reported herein. The load frequency is equal to 5 Hz to keep temperature levels close to the room

temperature. Prior to the experiment itself, the mechanical grips are always aligned. In the following, three configurations are analyzed, namely:

- a reference (R) configuration in which nominal parameters are considered (*i.e.,* bolt tension, clearance, surface finish),
- a more severe (S) configuration in which the surface of the external plates was sandblasted to increase the friction coefficient, the bolt tension being identical to R,
- the same configuration as the previous one, except that the bolt tension is reduced by 30 %. It is referred to as T.

Two cameras are used to monitor surfaces along two perpendicular directions (*i.e.,* normal and side views, see Figure 2). A random pattern is created by spraying black and white paint. Pictures are shot for a load increment of 5 kN upon loading and unloading for cycles 1, 5, 50, 100, 1 000, 10 000, 25 000, 50 000, 75 000 and 100 000. During these cycles, a stroke rate of 0.5 m / min is prescribed between two acquisitions. The pictures are subsequently correlated to determine displacement fields. Because of out-of-plane displacements in the normal direction, the only reliable information is given by the side view camera. It was checked a posteriori that along the optical axis of the side view camera the out-of-plane displacements were very small.

For the sake of simplicity, a finite-element based correlation technique is used in which 4 noded square elements are considered (Q4-DIC [29]). In the future, it is planned to use an enriched kinematics to account for displacement discontinuities [30, 31]. In the present case, 16-pixel elements are chosen. It corresponds to a good compromise between the standard displacement uncertainty and the spatial resolution (16 pixels $\leftrightarrow 550 - 600$ μm). The standard uncertainty level is obtained by following an a priori analysis [29] that consists is artificially moving the reference picture of the considered experiment by 0.5 pixel and measuring the displacement field. From the latter, the standard displacement uncertainty corresponds to the standard deviation of the measured field (here of the order of a few centipixels).

2.3 Validation of measurement procedure

For comparison purposes, an extensometer (gauge length: 50 mm) was used in the first test to measure the displacement between the composite and one of the aluminum alloy plates (Figure 2). On the opposite face, the displacement fields were followed by DIC. Contrary to the extensometer, DIC provides displacement *fields*. To compare the output of DIC and the extensometer, two zones (#2 and #3 boxes of Figure 3) in the vicinity of the bolt are considered. In each zone, the longitudinal displacements are averaged and denoted by $\langle U_{x2} \rangle$, and $\langle U_{x3} \rangle$, respectively. The displacement jump reads

$$\Delta U_x = |\langle U_{x3} \rangle - \langle U_{x2} \rangle| \tag{1}$$

This value is now compared with signals obtained by the extensometer. To compare the two signals, the physical size of one pixel needs to determined, and the frame of the assembly with respect to that of the picture. The user has to define (by mouse click) four points on the top edge of the assembly, and four points on the bottom part. With these 8 points two parallel lines are evaluated by least squares minimization and the distance between them corresponds to the width of the assembly expressed in pixels (*e.g.,* 437 pixels in Figure 3). An associated frame is then obtained. In this first case, the origin location is arbitrary. The procedure was repeated by the different authors and the corresponding uncertainty was less than 1 pixel. This low value was considered sufficient for the results to be reliable when expressed on a metric scale (*i.e.,* the physical size of one pixel is equal to 37.3 ± 0.1 μm).

Figure 4 shows comparisons for two different tests (a preliminary one and R). The two signals are close for the R configuration (a maximum difference of the order of 30 μm is observed), and coincident for a preliminary test. This difference cannot be caused by measurement uncertainties (well below the observed gap), nor due the conversion of pixels in mm. Last, out-of-plane displacements remained very low in that case. The only explanation can be understood by the fact the measurements are not performed on the same side (since the extensometer is too close to the surface to allow for an additional observation with a camera), and that a small asymmetry

occurred during the experiment. This was confirmed by the analysis of the normal view pictures. To fully validate this hypothesis, a third camera would have needed to monitor the other (normal) side.

From these preliminary results, it is concluded that the DIC measurements are trustworthy and they will be the only kinematic data used in the sequel. It is worth remembering that the extensometer cannot be used during the whole experiment. When cycling at a frequency of a few Hz, it should be unmounted. Therefore it is not possible to follow the total displacement jump by that measurement means alone. Further, high and low temperature tests were also performed (they are not reported herein). In both cases, the use of an extensometer was impossible. These are two additional advantages of using DIC in the present case.

2.4 Analysis of configuration R

Figure 5 shows the load / displacement jump loops for the experiment on configuration R. From now on, the displacement jump is defined as

$$\Delta U_x = \left| \frac{\langle U_{x1} \rangle + \langle U_{x3} \rangle}{2} - \langle U_{x2} \rangle \right| \tag{2}$$

where $\langle U_{x1} \rangle$, $\langle U_{x2} \rangle$, and $\langle U_{x3} \rangle$, are the mean longitudinal displacements of zones #1-3 of Figure 3. As the number of cycles increases, a stiffening of the assembly response is observed. The secant stiffness being defined by the maximum load amplitude divided by the corresponding displacement jump amplitude for each cycle (see Figure 8), an 80 % increase is observed in the present case. The permanent displacement jump also increases with the number of cycles. Conversely, the maximum displacement jump and the maximum hysteresis loop width decrease with the number of cycles. This analysis is made possible by the fact that the same reference image is considered in the DIC analysis for the whole series of pictures. The reasons for the change in the hysteresis loop location and width is a signature of surface modifications leading to a change of the friction coefficient, which almost invariably increases with the number of cycles [33]. This phenomenon may be attributed to plastic deformation of asperities

of the aluminum alloy surfaces, and/or micro-damage accumulation on the composite faces.

In the R configuration, the initial secant stiffness k is equal to 193 kN/mm. In the aeronautics industry, Huth's model [2] is commonly used to describe globally the behavior of various joints (*i.e.,* by modeling it as a spring with a given stiffness). The value of secant stiffness is compared with the prediction using Huth's formula

$$\frac{1}{k} = \xi \left(\frac{e_a + e_c}{2D}\right)^{2/3} \left(\frac{1}{e_a E_a} + \frac{1}{e_c E_c} + \frac{1}{e_a E} + \frac{1}{2e_c E}\right) \tag{3}$$

where E_a is Young's modulus of the external plates ($E_a = 71$ GPa), E_c the longitudinal Young's modulus of the composite plate ($E_c = 73.5$ GPa), E Young's modulus of the bolt ($E = 110$ GPa). In the present configuration, $\xi = 2.1$ [2] so that $k = 140$ kN/mm. The order of magnitude of the secant stiffness is correct. The main difference is related to the value of ξ, which is arbitrary (*i.e.,* independent of the details of the considered configuration). Furthermore, this simple expression does not account for the effect of pre-tension of the bolt, of the friction coefficient that may impact the response of the assembly. The aim of the following analyses is to adresse these issues.

3 Identification with the secant stiffness

In the sequel, displacement measurements on the side of the bolted sample are used to identify the friction coefficient f between aluminum alloy and composite plates. For the sake of simplicity, the only kinematic information used is the displacement jump as introduced in the previous section [Equation (2)]. When the physical size of one pixel is known (*i.e.,* it was determined by measuring the total thickness of the assembly in the picture, and for the R configuration the physical size of one pixel is 36 μm), the comparison is straightforward with the simulations. The unknown parameters are tuned by minimizing the difference between the measured and predicted secant stiffnesses of the assembly.

The numerical simulations are performed by COFAST, a finite element in-house code, which is dedicated to the simulations of assemblies with contact and friction in-

teractions [15]. It is based on a mixed domain decomposition approach that emphasizes the role of the contact zones that are modeled by interfaces. The iterative resolution scheme that is used corresponds to a two-step Uzawa algorithm associated with an augmented Lagrangian formulation of the problem. For symmetry reasons, only one quarter of the assembly is considered (Figure 6). The FE model contains 43 289 linear elements and 82 467 degrees of freedom. For the contact zones, unilateral contact with Coulomb friction [32] is considered. In the present case, it is assumed that the only non linearity is due to contact interactions. The various plates are assumed to behave elastically. A homogenized behavior is assumed for the layered composite. The tension in the bolt is accounted for as a first step of the simulation. It is prescribed by a relative axial motion between the nut and the screw. The amplitude of this motion is precalculated so that it generates the desired tension.

For each value of the friction coefficient, three cycles are performed numerically to reach a quasi steady state condition. The secant stiffness is measured from the last unloading part. The change of the former is shown in Figure 7 for different values of the friction coefficient f, the bolt tension T, clearance between the bolt and the holes in the plates. This first result shows that, as can be anticipated by accounting for Coulomb friction, the product fT is the only parameter that can be extracted from the secant stiffness. Furthermore, a linear fit described very well the correlation between the secant stiffness and the product fT. Consequently, the evaluation of the secant stiffness gives a direct access to the frictional load transmitted by the assembly.

Figure 8 shows a comparison of the load / displacement loops of two configurations (R and S). A very good agreement is obtained. This result shows that the secant stiffness as defined herein is a good parameter to choose for identification purposes. The *whole* loop is well described when the secant stiffness is correctly tuned. It is worth noting that when the first cycle is not considered, the value of the permanent displacement jump corresponding to a given number of cycles is not captured by the numerical procedure. Therefore, this offset is adjusted to draw the response of the simulation to account for the frictional state of a given number of cycles. For configuration R, the

tension after 100 000 cycles is measured to be $T = 21$ kN so that $f = 0.42$, and for configuration S, the initial tension is $T = 30$ kN, and thus $f = 0.48$. The fact that the surfaces are sandblasted is increasing the initial friction coefficient.

The change of the friction coefficient with the number of cycles is shown in Figure 9. Two cases are considered for the reference configuration (R). First, the tension T is assumed to be constant. As the number of cycles increases, the apparent friction coefficient increases too. Second, as mentioned above, the tension in the bolt was measured during the whole experiment. Therefore, it is possible to account for this change (decrease of T with N). A significant difference is observed when compared with the previous results. For the configuration R, the friction coefficient varies from 0.1 initially to 0.42 after 100 000 cycles. This type of trend is generally observed [33], in particular for more complex assemblies [14]. When the surface is sandblasted and the same initial tension is applied, the initial friction coefficient has a very high value (0.48). Moreover, as the number of cycles increase, there is only a small increase of the friction coefficient (from 0.48 to 0.61) compared to the previous case. Last, when the initial tension is decreased by a 30 % (reference T), the initial value (0.33) decreases but as the number of cycles increases, it reaches similar values (0.65) as configuration S. Last, it is worth noting that these values are in the same range as reported in Ref. [25].

Figure 10 shows the state of the surfaces at the end of the experiment for the T configuration. There is a clear degradation that can explain the qualitative increase of friction coefficient from the beginning and the end of the test. The zone in which a significant degradation is observed has a width approximately equal to the hole diameter.

4 Identification with full-field data

Up to now, the only information was provided by the measurement of the displacement jump, and the subsequent evaluation of the secant stiffness of the assembly. To validate the identification results, it is proposed to compare the displacement fields measured on the side face $\boldsymbol{U}_m$ with finite element simulations $\boldsymbol{U}_c$ of the same region of interest.

In that case, the two fields are compared up to a rigid body motion that may arise between the two situations. Consequently, the identification residual is defined as

$$\rho^2(f, \boldsymbol{U}_0, \boldsymbol{\Omega}) = \frac{1}{n} \sum_{i=1}^{n} \|\boldsymbol{U}_m(\boldsymbol{x}_i) - \boldsymbol{U}_c(\boldsymbol{x}_i, f) - \boldsymbol{U}_0 - \boldsymbol{\Omega} \times \boldsymbol{x}_i\|^2 \tag{4}$$

and its dimensionless counterpart η

$$\eta = \sqrt{\frac{\rho^2(f, \boldsymbol{U}_0, \boldsymbol{\omega})}{\frac{1}{n}\sum_{i=1}^{n} \|\boldsymbol{U}_m(\boldsymbol{x}_i) - \boldsymbol{U}_0 - \boldsymbol{\Omega} \times \boldsymbol{x}_i\|^2}} \tag{5}$$

where $\boldsymbol{U}_0$ is a rigid body translation, $\boldsymbol{\Omega}$ a rigid body rotation, and $\boldsymbol{x}_i$ any measurement point. As in the previous case, the pixel to mm conversion is needed. In the present case, there is an additional need for defining a common origin of both frames. This is made possible by following the same procedure as before, but to define two additional points corresponding to the left end of the composite plate. In Figure 3, the frame of the assembly is shown for the reference picture of configuration R. Once the frame was defined, the displacements of each node of the measurement mesh (Figure 3) obtained by any simulation are determined. The nodal displacements of the FE are used to be interpolated at the measurement nodes.

Figure 11 shows a comparison between the measured and simulated fields. The residual displacements are also shown. In the present case, the normalized residual is equal to 3 %. This value indicates that 97 % of the fluctuations of the displacement field is accounted for. For the longitudinal displacements, the discrepancies are mainly located along the plate surfaces. This is due to the fact that the measured displacements did not account for the discontinuity induced by the relative motions of the various plates. Apart from this difference, a very good agreement is observed. For the transverse displacement, the overall agreement is acceptable since the RMS difference is less than 10 μm. When compared to the measurement uncertainties, which were evaluated to be of the order of a few micrometers, it is concluded that the identified value of the friction coefficient is trustworthy. The remaining differences may be due to non-linear effects in the bearing zones (*e.g.,* plasticity and hardening of the aluminum alloy plates, damage of the composite plates).

The change of the dimensionless displacement residual η with the coefficient of friction f is shown in Figure 12. For the tested values, a clear minimum is obtained when $f = 0.2$ for the reference (R) configuration after 50 cycles of loading. Similarly, a value $f = 0.3$ is found for the T configuration after five cycles. Both values are obtained when the measured tension T is considered in the FE simulations. Moreover, these values are in very good agreement with the results found with the secant stiffness associated with the displacement jump measurement (see Figure 9). These two cases where considered because it was found that the secant stiffness was identical.

The present results (Figure 9 and 12) show that without the knowledge of T, it is impossible to correctly evaluate the friction coefficient with the two methods proposed herein. As a final illustration, two additional cases are considered. The first one corresponds to the reference configuration in which the tension is decreased (15.4 kN instead of 24.5 kN). A value of $f = 0.3$ minimizes the identification residual η. This value is consistent with a constant value of frictional load (4.75 ± 0.15 kN). Conversely, an augmented tension (of 50 %) is applied to the T configuration and a value of $f = 0.2$ minimizes the identification residuals, in agreement with a constant frictional force of 4.75 ± 0.15 kN.

5 Conclusions

It was proposed to use displacement fields measured by digital image correlation (DIC) to identify the frictional properties of a bolted assembly. The DIC procedure was first validated against extensometer measurements. The clear advantage of DIC is that it provides displacement *fields* as opposed to point data by using an extensometer. In the present work, only displacements obtained by analyzing pictures of the side view of the assembly are considered.

A first identification route consists in evaluating the secant stiffness in a load / displacement jump curve. It was shown that there exists a one-to-one (linear) relationship between the secant stiffness and the frictional load transmitted by the assembly. Therefore, if the tension in the bolt is known, then it is possible to identify the friction

coefficient. This type of identification procedure was then used to study the change of the friction coefficient with the number of cycles for three different configurations. For the reference configuration, a logarithmic model describes well the change of the friction coefficient with the number of cycles. For a sandblasted surface with the same initial tension, the friction coefficient increases only mildly with the number of cycles. For the same type of surface preparation with a reduced tension, the initial value of the friction coefficient is less than in the previous case, however, when the number of cycles increases, it reaches similar levels as in the previous case.

A second route, which is more involved, compares the measured displacement *fields* with the computed ones for different tensions and friction coefficients. It was used herein to validate the first route that is less time consuming once the (linear) relationship between the secant stiffness and the frictional load is established. In particular, it was shown that the sole knowledge of kinematic data is not sufficient to identify the friction coefficient and the bolt tension. The use of normal views, once out-of-plane displacements are account for (*e.g.,* by resorting to stereocorrelation or 3D-DIC [34]), is one possible way of addressing this last point. The next step is to extend the analysis to other joints.

Acknowledgements

The support of this research by Airbus is gratefully acknowledged.

References

1. M. A. McCarthy, C. T. McCarthy and G. S. Padhi, A simple method for determining the effects of bolt-hole clearance on load distribution in single-column multi-bolt composite joints, *Comp. Struct.* **73** (2006) 78-87.
2. H. Huth, Influence of Fastener Flexibility on the Prediction of Load Transfer and Fatigue Life for Multiple-Row Joints, in: *Fatigue in mechanically fastened composite and metallic joints*, J. M. Potter, ed., (ASTM, Philadelphia, PA (USA), 1985), **STP 927** 221-250.
3. M. Cloarec, P.-A. Boucard, L. Champaney, S. Guinard and J. Sen Gupta, Study for design and identification of a bolted joint model, *Proceedings Complas IX - 9th International Conference on Computational Plasticity*, (2007), 889-892.
4. J. Bortman and B.A. Szabo, Nonlinear models for fastened structural connections, *Comput. Struct.* **43** (1992) 909-923.
5. J. Kim, J. Yoon and B. Kang, Finite element analysis and modeling of structure with bolted joints, *Appl. Math. Modelling* **31** (2007) 895-911.
6. J. Ekh and J. Schön, Load transfer in multirow, single shear, composite-to-aluminium lap joints, *Comp. Sci. Tech.* **66** (2006) 875-885.
7. J. Änggård, *Parametric study of lap joint, lap joint load transfert and stress characteristics*, (Report FFA TN 2000-44, 2000).
8. J. Esquillor, J. Huet and F. Lachaud, Modélisation par éléments finis d'un assemblage aéronautique en simple cisaillement, *Proc. 17^e Congrès Français de Mécanique*, 2005.
9. K. I. Tserpes, P. Papanikos and T. Kermanidis, A three-dimensional progressive damage model for bolted joints in composite laminates subjected to tensile loading, *Fat. Fract. Eng. Mat. Struct.* **24** [10] (2001) 663-675.
10. M. A. McCarthy, C. T. McCarthy, V. P. Lawlor and W. F. Stanley, Three-dimensional finite element analysis of single-bolt, single-lap composite bolted joints: Part I–model development and validation, *Comp. Struct.* **71** (2005) 140-158.
11. C. T. McCarthy and M. A. McCarthy, Three-dimensional finite element analysis of single-bolt, single-lap composite bolted joints: Part II–effects of bolt-hole clearance, *Comp. Struct.* **71** (2005) 159-175.
12. Y. Xiao and T. Ishikawa, Bearing strength and failure behavior of bolted composite joints (part II: modeling and simulation) *Comp. Sci. Tech.* **65** [7-8] (2005) 1032-1043.
13. F.-X. Irisarri, N. Carrère and J.-F. Maire, Simulation of the Behaviour of Bolted Joints in composites Structures, *Proc. JNC 2007*, 2007.
14. A. Caignot, P. Ladevèze, D. Néron and J.F. Durand, Virtual testing for the prediction of damping in joints, *Eng. Comput.*, **5**, (2010) 621-644.
15. C. Blanzé, L. Champaney, J.Y. Cognard and P. Ladevèze, A modular approach to structure assembly computations - Application to contact problems, *Eng. Comput.* **13** (1996) 15-32.

16. P.A. Boucard and L. Champaney, A suitable computational strategy for the parametric analysis of problems with multiple contact, *Int. J. Num. Meth. Eng.* **57** (2003) 1259-1281.
17. L. Champaney, P.A. Boucard and S. Guinard, Adaptive multi-analysis strategy for contact problems with friction, *Comput. Mech.* **42** (2007) 305-316.
18. R. Starikov, *Mechanically fastened joints: critical testing of single overlap joints*, (Report FOI-R–0441–SE, 2002).
19. R. Starikov and J. Schön, Experimental study on fatigue resistance of composite joints with protudring-head bolts, *Comp. Struct.* **55** (2002) 1-11.
20. Y. Xiao and T. Ishikawa, Bearing strength and failure behavior of bolted composite joints (part I: Experimental investigation), *Comp. Sci. Tech.* **65** [7-8, June] (2005) 1022-1031.
21. R. Starikov, Fatigue behaviour of mechanically fastened aluminium joints tested in spectrum loading, *Int. J. Fat.* **26** (2004) 1115-1127.
22. J. Ekh, J. Schön and L. Gunnar Melin, Secondary bending in multi fastener, composite-to-aluminium single shear lap joints, *Comp. Part B* **36** (2005) 195-208.
23. R. Starikov and J. Schön, Local fatigue behaviour of CFRP bolted joints, *Comp. Sci. Tech.* **62** (2002) 243-253.
24. J. Schön, Coefficient of friction of composite delamination surfaces, *Wear* **237** (2000) 77-89.
25. J. Schön, Coefficient of friction for aluminum in contact with a carbon fiber epoxy composite, *Tribology International* **37** (2004) 395-404.
26. V. P. Lawlor, M. A. McCarthy and W. F. Stanley, An experimental study of bolt-hole clearance effects in double lap, multi-bolt composite joints, *Comp. Struct.* **71** (2005) 176-190.
27. R. Starikov and J. Schön, Quasi-static behaviour of composite joints with protruding-head bolts, *Comp. Struct.* **51** (2001) 411-425.
28. M. E. Kartal, D. M. Mulvihill, D. Nowell and D. A. Hills, Determination of the Frictional Properties of Titanium and Nickel Alloys Using the Digital Image Correlation Method, *Exp. Mech.* **51** (2011) 359-371.
29. G. Besnard, F. Hild and S. Roux, "Finite-element" displacement fields analysis from digital images: Application to Portevin-Le Chatelier bands, *Exp. Mech.* **46** (2006) 789-803.
30. J. Réthoré, S. Roux and F. Hild, From pictures to extended finite elements: Extended digital image correlation (X-DIC), *C. R. Mécanique* **335** (2007) 131-137.
31. J. Réthoré, F. Hild and S. Roux, Shear-band capturing using a multiscale extended digital image correlation technique, *Comp. Meth. Appl. Mech. Eng.* **196** [49-52] (2007) 5016-5030.
32. C. A. de Coulomb, *Théorie des machines simples, en ayant égard au frottement de leurs parties et à la roideur des cordages*, (Recueil des savants étrangers de l'Académie Royale des Sciences, Paris (France), 1781).

33. D. A. Hills and D. Nowell, What features are needed in a fretting fatigue test?, *Tribology Int.* **42** (2009) 1316-1323.

34. M. A. Sutton, J.-J. Orteu and H. Schreier, *Image correlation for shape, motion and deformation measurements: Basic Concepts, Theory and Applications*, (Springer, New York, NY (USA), 2009).

List of Figures

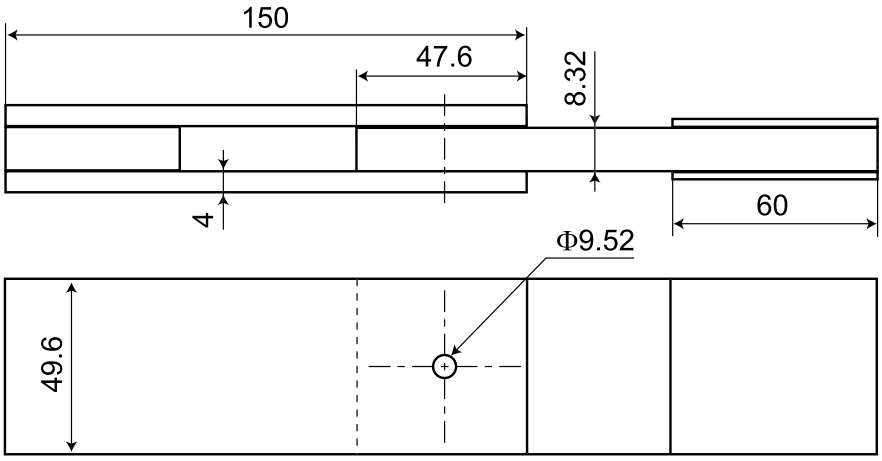

Fig. 1 Double lap joint sample with a single bolt. The two external plates are made of aluminum alloy, and the central plate is made of carbon / epoxy. The dimensions are expressed in mm.

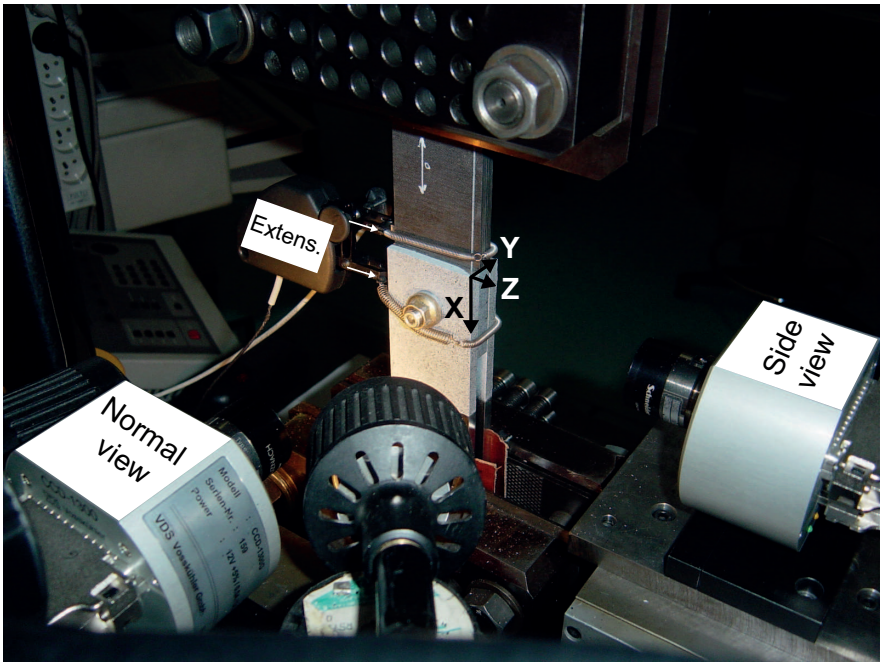

Fig. 2 Experimental set-up. The sample is fixed in mechanical grips. Two cameras are used to monitor the motion of prepared surfaces (random texture) from two angles of view (side and normal). Only the side view pictures ($X-Y$ plane) are used herein. The extensometer was used to measure the displacement jump (see white arrows) of the first loading cycles. It had to be removed when subsequent cyclic loads were applied.

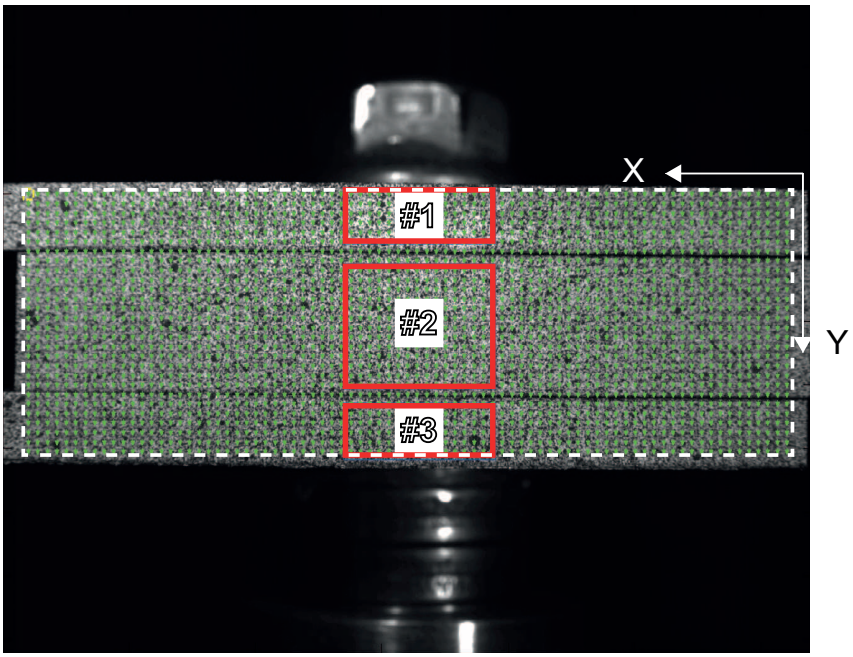

Fig. 3 Example of a reference picture. The nodes of the measurement mesh (Q4-DIC) are shown, the element size is equal to 16 pixels (1 pixel $\leftrightarrow$ 37.3 μm). The three red boxes depict the regions over which the measured displacements are averaged to determine the displacement jump ΔU_x [see Equations (1) and (2)]. The dashed box corresponds to the ROI that was used to compare measured and simulated displacement fields.

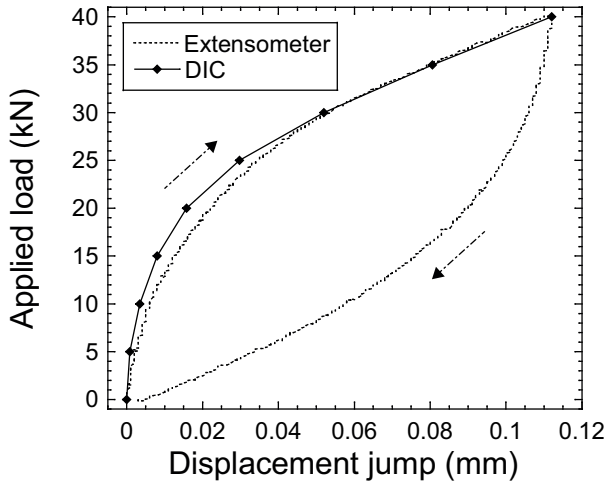

(a)

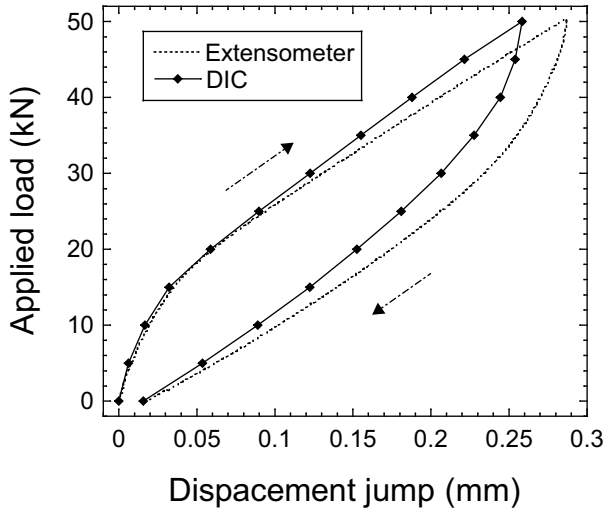

(b)

Fig. 4 Comparison between the signals of the extensometer and DIC. Two configurations (preliminary (a) and reference R (b)) are used.

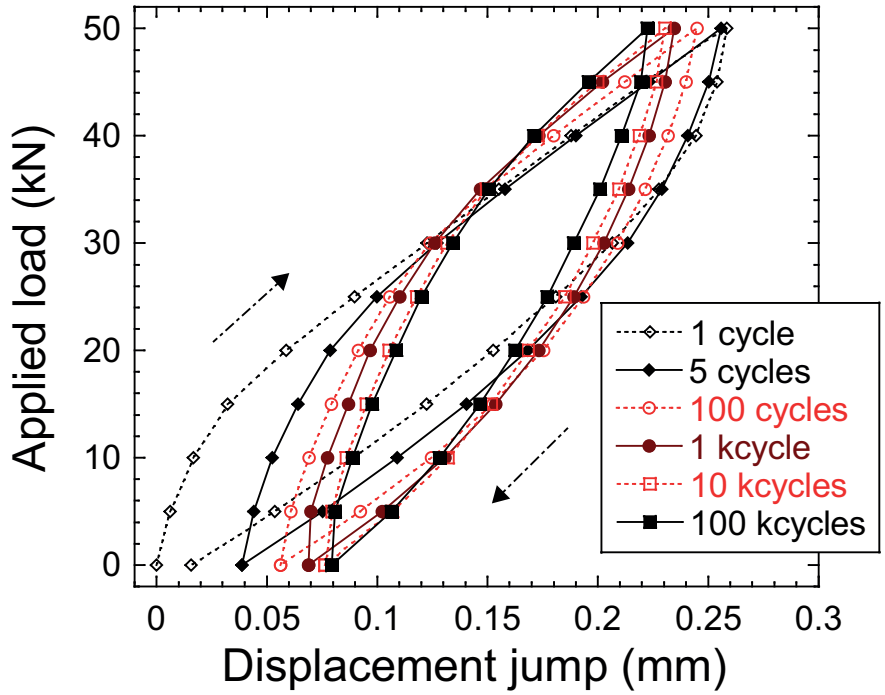

Fig. 5 Load vs. displacement jump for different cycles of the test on the reference (R) configuration.

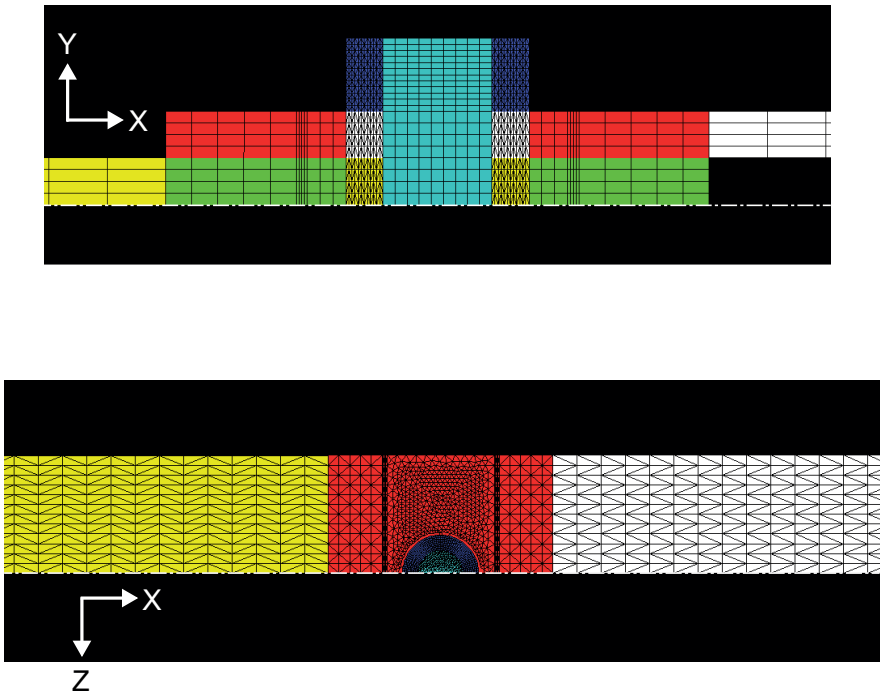

Fig. 6 Numerical model of one quarter of an assembly. Symmetry conditions are used. The dashed lines indicate symmetries.

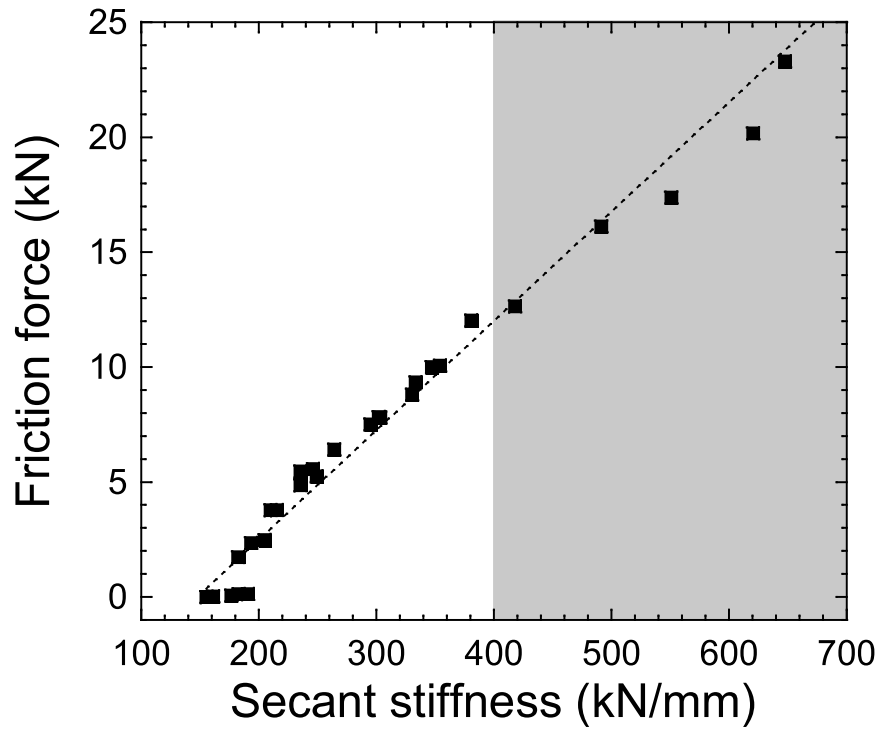

Fig. 7 Change of the secant stiffness as a function of the friction force fT in the the bolt for various conditions. The dashed line shows a linear interpolation of all the results. The gray shaded area is not reached with the experiments reported herein.

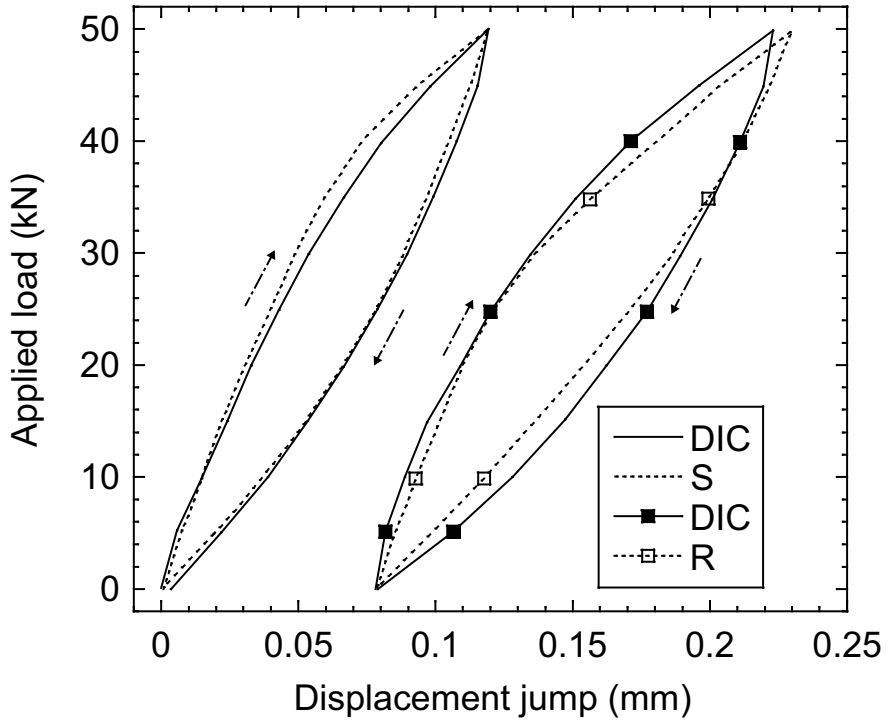

Fig. 8 Comparison between measured and identified load vs. displacement jump loops for two (R and S) of the studied assemblies.

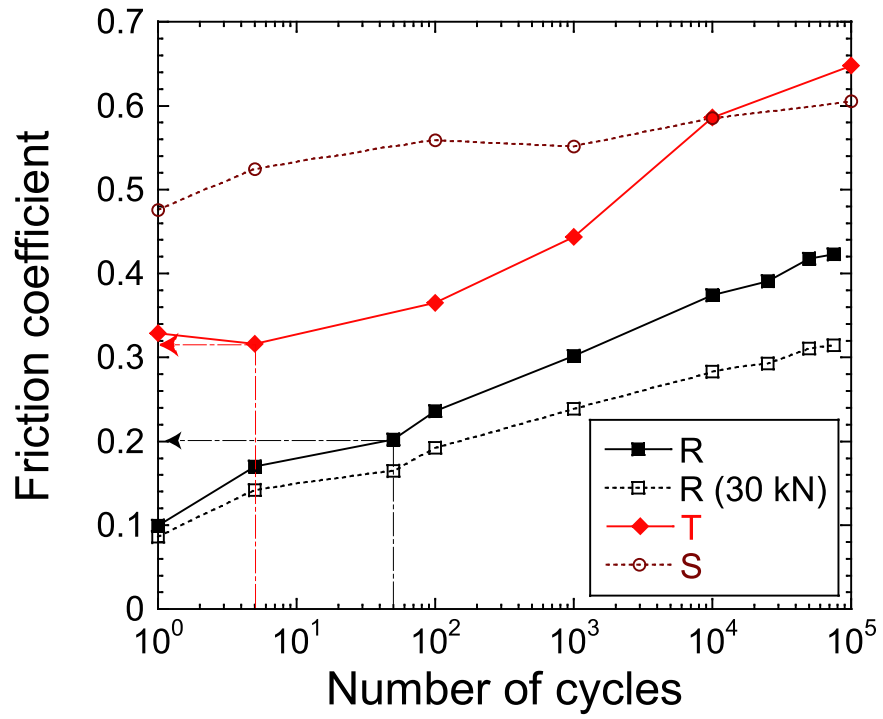

Fig. 9 Change of the identified friction coefficient f with the number of cycles for the three studied configurations. For the reference configuration (R) a comparison is given by assuming that the bolt tension is constant (30 kN). A significant difference is observed. The two marked cases are used for comparison purposes with a more detailed analysis of the displacement field (Figure 12)

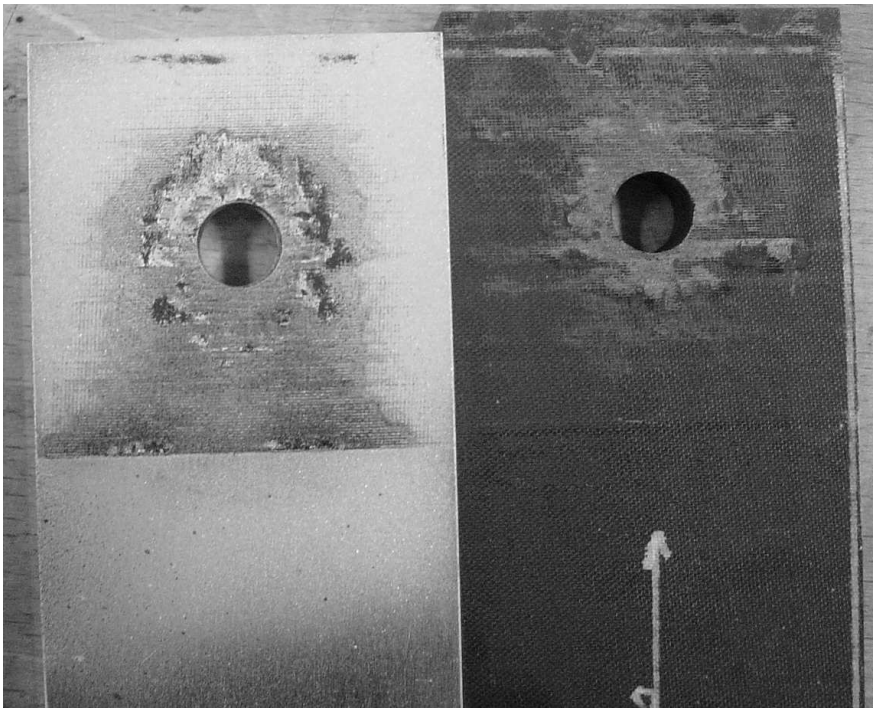

Fig. 10 Observation of the worn surfaces after 100 000 cycles for the T configuration. The width of the plates is equal to 49.6 mm.

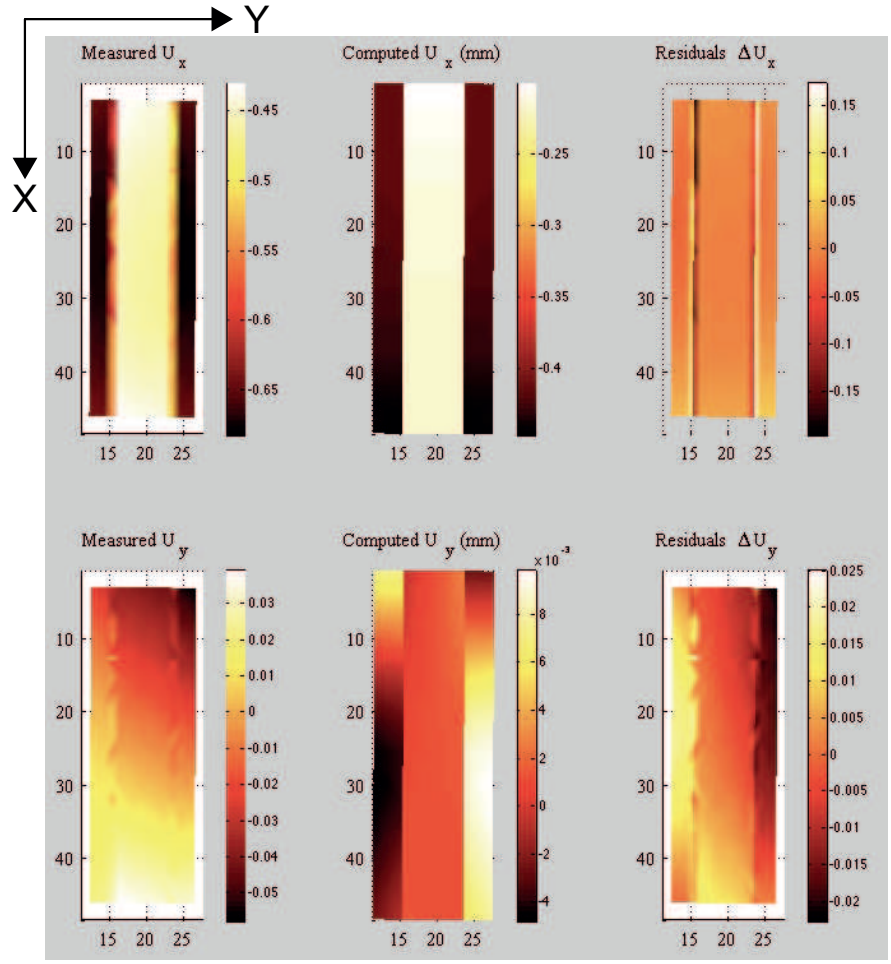

Fig. 11 Comparison between measured and identified displacement fields for configuration R after 10 000 cycles. The corresponding difference is also shown when rigid body motions are accounted for. All displacements are expressed in mm.

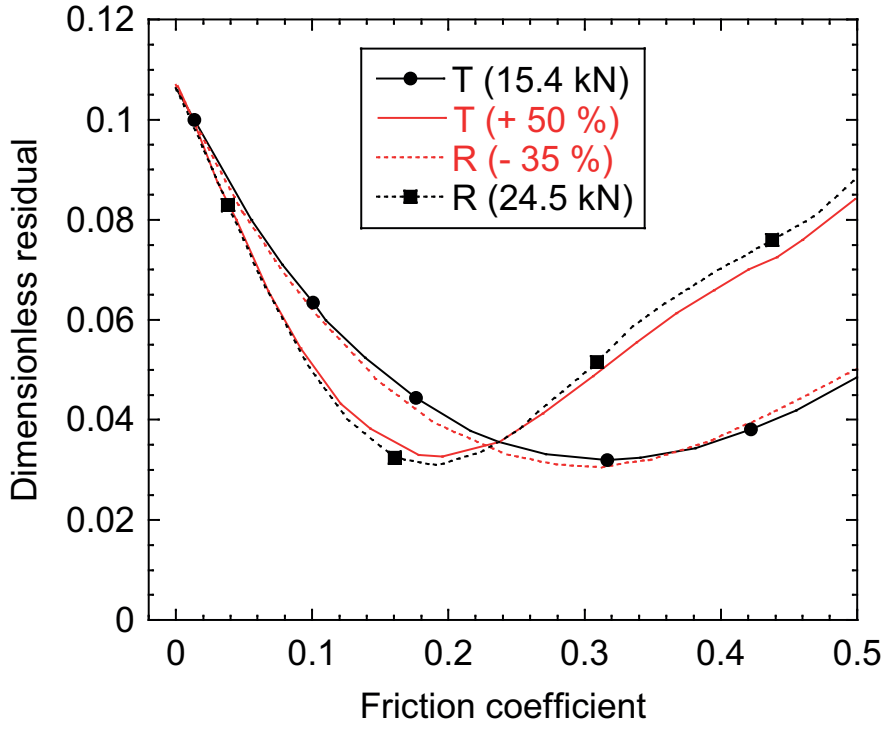

Fig. 12 Change of the dimensionless identification residual η with the friction coefficient f for the two configurations (R for 50 cycles of loading, and T for 5 cycles of loading) leading to the same secant stiffness. The minimum values are in very good agreement with the results shown in Figure 9. A comparison is given for the reference configuration with a reduced tension of 35 %, and the T configuration with an increased tension of 50 %.